EEET ECOLOGICAL ENGINEERING & ENVIRONMENTAL TECHNOLOGY

Ecological Engineering & Environmental Technology, 2026, 27(1), 65–84
https://doi.org/10.12912/27197050/214690
ISSN 2719–7050, License CC-BY 4.0

Received: 2025.10.23
Accepted: 2025.12.15
Published: 2026.01.01

Assessment of landslide risks in the western High Atlas of Morocco following the El Haouz earthquake, using the analytical hierarchy process and multi-criteria geographic information system

Fatima-Ezzahrae Allaki[1*], Kaoutar Bargach[1], Abdelmounim Qarbous[2]

[1] Geo-Biodiversity and Natural Patrimony Laboratory (GEOBIO), Scientific Institute, Mohammed V University in Rabat, Morocco
[2] Department of Geology, Regional Center for Education and Training Professions, Rabat, Morocco
* Corresponding author's e-mail: fatimaezzahrae_allaki@um5.ac.ma

ABSTRACT

The aim of this study is to delineate landslide susceptibility maps for western High Atlas region using the analytical hierarchy process (AHP) method. Several parameters considered for mapping the landslide susceptibility, including slope, lithology, curvature, fault density, aspect, hydrographic network, and seismic magnitudes. Thematically organized layers and distributed maps of all parameters were generated within a GIS environment. To assign appropriate weights, the significance of these thematic factors layers in landslide occurrence was determined by comparing them with Preferred Landslide Model from the USGS database and on Field trip in the studied sector. The landslide susceptibility model was then elaborated by a weighted sum method in a GIS platform after being analyzed using the AHP analysis. The classification of the landslide susceptibility map was performed using the data presented in this study as very high (5.30%), high (15.10%), moderate (59.41%), low (14.91%), and very low (5.27%). The combination of satellite data and the landslide susceptibility map revealed that the moderate to very high susceptibility zones contained 79.81% of the total study area (32 123,1 km^2). The findings of this study are useful for identifying landslide-prone areas in the region, offering a crucial reference for future construction and planning following the 2023 Al Haouz seismic disaster. Furthermore, this landslide susceptibility analysis contributes valuable data to research concerning similar geological sites.

Keywords: landslides risk, analytic hierarchy process, GIS-multicriteria, western High Atlas, Al-Haouz earthquake.

INTRODUCTION

Positioned geographically within the NW-SE trending convergence zone of the African and Eurasian tectonic plates, Morocco is characterized by seismic activity generally classified as low to moderate (Cherkaoui and El Hassani, 2015). However, this geodynamic context endows the country with significant exposure to seismic risks, the consequences of which can be devastating (Cherkaoui et al., 2017). The Al Haouz event of September 8, 2023, at 22:11 (GMT), devastated the Al Haouz region. According to the USGS (United States Geological Survey), it registered a magnitude of 6.8 Mw and occurred at a depth of 19.0 km. This is considered the most significant seismic event of the last century in the area. The epicenter, as reported by the National Institute of Geophysics of the National Center for Scientific and Technical Research (CNRST), was located in the commune of Ighil, Al Haouz province, approximately 70 km southwest of the city of Marrakech. The human toll was tragic, resulting in over 2,960 fatalities and 6,125 injured. Although the damage caused by the earthquake was substantial, subsequent gravitational movements (landslides, collapses, rockfalls, and ruptures) were triggered, amplifying the destruction of infrastructure, particularly roads and rural communities. Structural analysis indicates that

the initiation of landslides was likely facilitated by the reactivation of neotectonic structures responsible for the current seismicity in the High Atlas (Asebriy and Cherkaoui, 1995; El Fellah et al., 1996). Characterizing the regional crustal stress field within the context of the Africa-Eurasia convergence aids in identifying the faults most likely to trigger seismic activity, which subsequently induces structural changes and rock slippage (Levandowski, 2023). Seismic activity has the potential to generate a reorganization of internal stress fields and the mechanical properties of rocks, potentially leading to progressive or abrupt failures (Abdallah et al., 2013). Furthermore, the specific distribution of rock masses in the western High Atlas region – characterized by high mountains and steep slopes – makes this area susceptible to significant landslide risks, particularly in tectonically active zones (Keefer, 1984; Azzouz et al., 2002; Sassa et al., 2007; Havenith

Table 1. Previous studies on landslides conducted at the international and Moroccan levels

Author	Year	Approach	Parameter	Comment	Results
Thiery & Terrier	2018	Numerical Approaches for Susceptibility (Alternative Approaches)	Topography, Lithology, Geological structure, Hydrology & Hydrogeology, Land Use/LandCover, Vegetation Cover, Historical phenomena	Approach relies on generic predictive models and does not specifically integrate seismic parameters, which are essential in a seismogenic context.	Satisfactory
Serkhane et al.	2024	Frequency Ratio (FR) Weight of Evidence (WoE)	Slope, Aspect, Lithology Distance to Drainage Network, Rainfall, Distance to Faults, Distance to Roads	These methods are limited to observed spatial relationships and do not incorporate dynamic factors such as seismic stresses, limiting their immediate post-seismic applicability.	Satisfactory
Liu et al.	2024	Analytical Hierarchy Process (AHP)	Land Use (or Land Use/Land Cover), Lithology, Soil, River Density, Curvature, Aspect, Slope, Elevation	This method relies heavily on subjective expert judgments and does not systematically incorporate quantitative seismic data in its comparison matrices.	Assumption
Rivera et al.	2025	Analytical Hierarchy Process (AHP)	Distance to population centers, Distance to roads, Land use, Precipitation, Drainage density, Distance to faults, Topographic Wetness Index, Relative relief, Profile curve, Slope angle, Elevation		Assumption
Amaya et al.	2014	Geographic information system (SIG) & Remote sensing.	Lithology, Slope, Fracturation	These approaches, although powerful for spatial analysis, focus on surface characterization without modeling the dynamic interaction between seismic ground motions and slope stability.	Assumption
El Qayedy et al.	2006	Remote sensing (satellite imagery) and field spectral measurements (spectroradiometry).	Données ASTER		Assumption
El Aaggad et al.	2014	Detailed mapping of landslides	Topography, Lithology, Geological Structure, Vegetal Cover.	This descriptive method lacks predictive modeling and does not allow for regional extrapolation of susceptibilities in a seismic context.	Assumption
Labriki et al.	2025	Differential Synthetic Aperture Radar Interferometry (DInSAR).	Radar imagery for D-InSAR analysis and seismic data.	This method remains a reactive, post-event approach without integrated predictive capability for proactive risk assessment.	Satisfactory
Ennassiri et al.	2021	Multi-criteria analysis	Vulnerability of Buildings & Seismic Hazard, Built Vulnerability & Seismic Hazard	This approach, although comprehensive in its vulnerability assessment, does not explicitly address the seismic triggering of landslides and remains focused on the stakes rather than the geodynamic processes.	Assumption

and Bourdeau, 2010). Despite the Al Haouz event – one of the most powerful earthquakes recorded in Morocco in recent decades – striking the western High Atlas region on September 8, 2023, few systematic studies have addressed landslide risk within a seismotectonic context (Labriki et al., 2025). This oversight is scientifically significant, considering the established role of ground movements in amplifying seismic damage, especially in mountainous and structurally complex environments. Prior research concerning landslide assessment (Table 1) has largely employed diverse methodologies, incorporating geological, topographical, and environmental factors. For example, Thiery and Terrier (2018) utilized numerical approaches based on topography, lithology, and hydrology, whereas Serkhane et al. (2024) applied statistical methods such as frequency ratio (FR) and weight of evidence (WoE). Other studies, including those by Liu et al. (2024) and Rivera et al. (2025), employed the AHP to weight various morphological and land use parameters. However, the majority of these works rely on predictive models or expert judgment, and few have explicitly integrated seismic parameters into susceptibility assessments. Contributions such as that of Ennassiri et al. (2021) focused on the seismic vulnerability of buildings but did not explicitly link seismogenic activity to landslide triggers. Furthermore, local studies conducted in Morocco, such as those by Amaya et al. (2014) and El Aaggad et al. (2014), were limited to the descriptive mapping of ground movements, without multi-criteria modeling in a seismic context. However, efforts made over the past 20 years, notably in the United States, have taken advantage of improved landslide event data, technology, and geospatial information to develop more accurate and precise national and global landslide susceptibility maps. Comprehensive post-seismic assessments remain inadequately addressed in the Moroccan context. This deficiency constrains the understanding of regional dynamics in mountainous areas subjected to seismic motion, hindering the development of accurate risk scenarios. The Al Haouz earthquake, therefore, offers an unparalleled opportunity to investigate the interaction between strong ground motion and lithological, topographical, and structural factors that define landslide susceptibility patterns across diverse geological settings. Therefore, to address this deficiency and improve the dependability of landslide susceptibility maps within seismically active areas, the formulation of an integrated approach – combining geological, seismological, and remote sensing data using a technique like the AHP – is deemed crucial. This investigation primarily intends to produce an initial detailed susceptibility map for the mass wasting events linked to the 2023 Al Haouz earthquake and to evaluate their spatial arrangement with respect to the dominant geological, tectonic, and seismological controlling variables. By doing so, this work not only contributes to a deeper comprehension of how mountain slopes in the Atlas range respond to seismic activity but also delivers vital information for refining seismic risk evaluation in Morocco (Nouayti et al., 2024; Ziraoui et al., 2024), a nation increasingly facing the simultaneous effects of seismotectonic hazards (Lewandowski, 2023; Nouayti et al., 2024; Qarbous et al., 2025).

GEOLOGICAL SETTING

Our study area is situated in the western High Atlas (WHA), which constitutes the highest and westernmost segment of the Moroccan Atlas Mountain range (Figure 1). Serving as a critical natural laboratory for analyzing tectonic processes, geomorphology, and natural hazards, this region is precisely delineated by its geographical limits: the Al Haouz plain and the imperial city of Marrakech bound it to the north; the Souss Basin and its eastward extension towards the Ouarzazate Basin define the south; the Atlantic Ocean and the western Meseta form the boundary to the west; and the central High Atlas (CHA) lies to the east. The WHA is characterized by its high elevations and a narrow profile compared to the central High Atlas. Its lithology (Figure 1) is predominantly composed of Precambrian and Paleozoic rocks, specifically schists, gneisses, and granites. Triassic locally and directly overlies these basement rocks through Cretaceous sediments. Triassic rocks, comprising sandstones and evaporites, are frequently restricted to narrow grabens, such as the Ourika, Telouet, and Taroudant corridors (Baudon et al., 2009; Domènech, 2015; El Arabi et al., 2003).

The Paleozoic basement of the WHA is segmented into three distinct zones by longitudinal faults: the Axial Zone, and the northern and nouthern Subatlasic Zones. Extensive basement outcrops define the Axial Zone, where Mesozoic cover is limited to Triassic deposits preserved

within tilted half-basins (Qarbous et al., 2003a; Domenech et al., 2015). The basement reaches a considerable thickness of nearly 5 km, encompassing volcano-sedimentary formations that span from the upper Ediacaran to the Visean-Namurian (Schaer, 1964; Michard et al., 2010).

Structurally, the WHA was impacted by the Hercynian compressional phase. The resulting deformation was primarily focused along the Tizi n'Test dextral wrench fault (Figure 1) (Mattauer et al., 1972; Petit, 1976; Proust et al., 1977). Notably, the effects of this orogeny are significantly more pronounced in the WHA basement compared to the adjacent Anti-Atlas (Mattauer et al., 1972; Michard et al., 2010). Extensional tectonics, linked to the fragmentation of Pangaea since the Permian period, led to the development of a rift basin. This basin was predominantly active during the Triassic and Jurassic (Beauchamp et al., 1996; Laville and Pique, 1991; Mattauer et al., 1977). The northwest-southeast (NW-SE) oriented extension generated and subsequently reactivated pre-existing normal faults trending from northeast-southwest (NE-SW) to east-northeast-west-southwest (ENE-WSW) (Petit et al., 1985; Medina and Errami 1996, Qarbous et al., 2003).

Triassic syn-rift deposits, which may achieve thicknesses of approximately 5 km within the Argana Corridor, are capped by lava flows belonging to the Central Atlantic Magmatic Province (CAMP), dated at about 201 Ma (Olsen et al., 2003; Blackburn et al., 2013). Subsequently, the uplift of the west Moroccan Atlas during the middle-upper Jurassic resulted in the erosion of the previously accumulated Triassic-Liassic sediments (Ghorbal et al., 2008; Domenech et al., 2016). Beginning in the upper Cretaceous, the global compressional stress field associated with the Africa-Eurasia convergence caused the inversion of the High Atlas rifts (Frizon de Lamotte et al., 2000; Froitzheim et al., 1988; Teixell et al., 2003). The structural evolution during this inversion was dominated by reactivation of inherited tectonic structures (e.g., Fraissinet et al., 1988; Morel et al., 2000; Qarbous et al. 2008, Amrhar, 2002, Ibouh and Chafiki, 2017). As discussed in Qarbous et al. (2025), the first phase was NW-SE to NNW-SSE direction is Mio–Pliocene in age (Dutour and Ferrandini, 1985; Fraissinet et al., 1988; Morel et al., 2000; Amrhar, 2002); The second is N-S to NNE–SSW direction but is controversial in age: upper Cretaceous (Mattauer et al., 1977; Froitzheim et al., 1988; Laville and Pique, 1991; Ibouh and Chafiki, 2017), Oligocene (Jenny, 1983; Brede et al., 1992), upper Cretaceous to Oligocene (Medina, 1994), Quaternary (Fraissinet et al., 1988; Morel et al., 2000), and Maestrichtian to

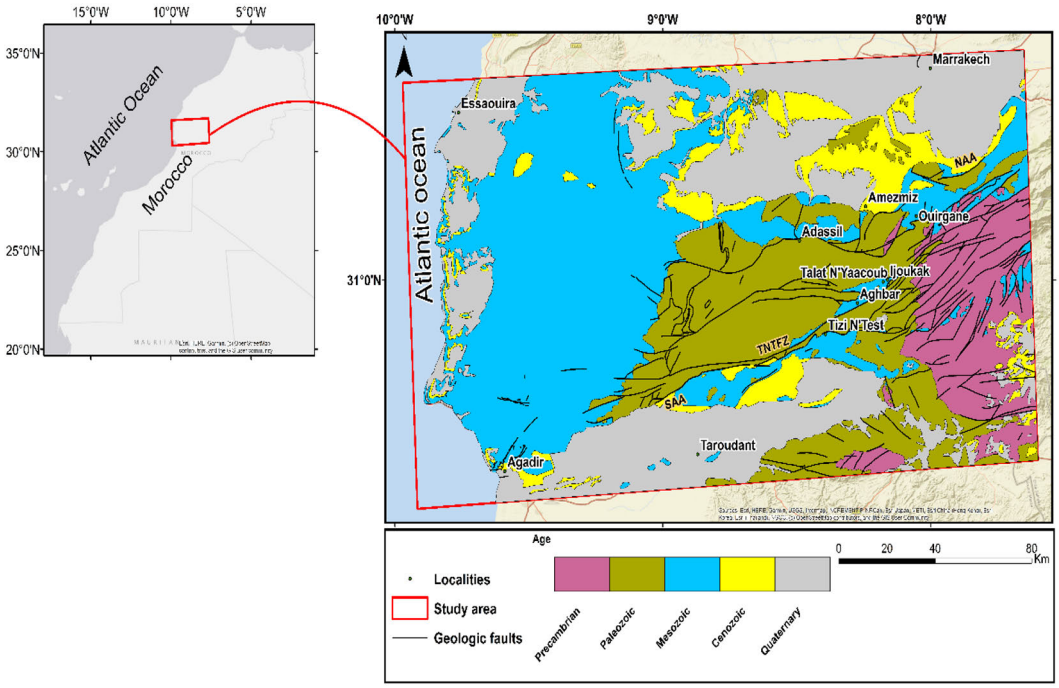

Figure 1. The geological sketch up of study area. (TNTFZ: Tizi N' Test fault zone. SAA: South Atlasic Accident. NAA: North Atlasic Accident)

Oligocene (Amrhar, 2002). Other studies show that this submeridian phase rotates locally from NNE–SSW to NNW–SSE commencing in the Maestrichtian–lower Paleocene and lasting until the Neogene (Fekkak et al., 2018).

MATERIALS AND METHODS

Study area selection

The delineation of the study area was expanded to include the sectors most susceptible to the secondary effects of the September 8, 2023 Al Haouz earthquake on slope stability. This choice is justified by the convergence of three major factors: geological, seismological, and topographical. From a seismotectonic perspective, the region is located in an active domain, where the earthquake reactivated neotectonic faults (Yeck et al., 2023; Bao et al., 2025), thereby weakening rock masses over a vast area. Topographically, the area is characterized by the high relief of the western High Atlas, with steep slopes where gravity amplifies the destabilizing effect of tremors (Azzouz et al., 2002). By targeting an extended area exhibiting these characteristics, the study aims to capture the diversity and magnitude of induced ground movements, such as rockfalls and rotational landslides. This approach is essential for establishing accurate hazard mapping and understanding failure mechanisms at a regional scale. The confluence of recent seismicity and neotectonic stresses in this high-mountain relief establishes the zone as both a major geological risk epicenter and a crucial natural laboratory for the study of post-seismic landslides across the western High Atlas.

Methodology

The methodology employed in this research is detailed in the flowchart (Figure 2). The core goal was to map landslide susceptibility, which was achieved using an integrated approach that combined geographic information systems (GIS), remote sensing, and the AHP. To develop the susceptibility map, a multi-parametric database was utilized, consisting of satellite imagery, geological and topographic maps, and seismological data. The foundational map of the study area was created by digitizing a geological map originally scaled at 1:1,000,000. Seven thematic layers – lithology, fracturation density, slope, aspect, curvature, hydrographic network, and magnitude interpolation – were used for the landslide susceptibility mapping. Fracturation densities were prepared using three methods of linear density analysis in ArcGIS 10.8 and Envi 5.6 softwares.

Fracturation

Lineament extraction

A Landsat 8 OLI/TIRS image, specifically dated May 19, 2024, was downloaded from the the United States Geological Survey (USGS) online

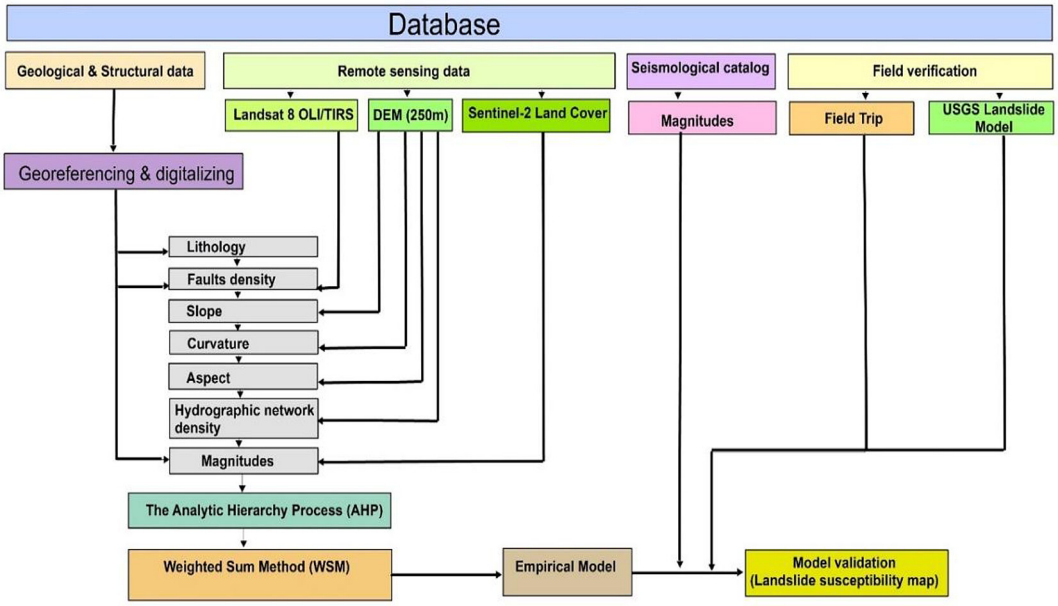

Figure 2. Methodological flow chart

database (https://earthexplorer.usgs.gov). This orthorectified image, projected in WGS84 (UTM zone 30N), was utilized to map the sector's lineaments using detection algorithms. This process involved applying the empirical Moore method (Moore, 1983), in line with the methodology previously employed by (Timoulali et al. 2019; Redouane et al. 2022). The image was processed using the ENVI Classic 5.6 platform according to the following steps: (1) preprocessing involving atmospheric and radiometric corrections; (2) principal component analysis (PCA) on 11 bands to enhance image quality; (3) application of convolution filters to extract features; (4) use of directional filters to detect edges with a typical angle of 60°; (5) application of Gaussian high-pass filters to accentuate fine details – this enhancement was performed by accessing the "enhance" option, then selecting the "filter" class and "sharpen" (linear 2% and grayscale 0-255); (6) region of interest (ROI) involving the drawing of lineaments using the polyline tool for more detailed analysis; (7) transfer of Landsat 8 OLI/TIRS lineaments to ArcMap 10.8 for better management and visualization.

Digital elevation model lineament extraction

To analyze the major tectonic features, the shuttle radar topographic mission (SRTM) digital elevation model (DEM), which has a 250-meter resolution and was downloaded from the aforementioned USGS website, was employed.Lineaments were extracted using ArcGIS 10.8 software, specifically via the "hillshade" tool within the "spatial analysis" extension in Arc Toolbox. This tool generates a shaded relief from a raster by considering the angle of the light source and projected shadows.Following the methodology of (Makkaoui et al. 2024), the shading parameters included an altitude of 45° and azimuth settings of 315°, 225°, 135°, and 45°. These settings were used to identify lineaments in the respective directions: NE-SW to N-S; N-S to E-W; NE-SW, and NW-SE. A Z-factor of 0.00001036 was applied to ensure the measurement units were correctly adjusted for the study area.

Geological faults

The geological faults used in this study were sourced and digitized from several existing cartographic documents: the Agadir map (1:50,000; Ambroggi, 1963), the Argana Corridor map (1:100,000; Tixeront, 1973), and the Taghazout map (1:100,000; Choubert, 1971). These core documents were supplemented by the comprehensive geological map of Morocco (1:1,000,000; Geological Service, 1985; Notes et Mémoires series, No. 260). The methodology began with the georeferencing of all maps. Subsequently, the primary faults were digitized in ArcGIS 10.8 using the polyline tool, with classification based on their type. After extracting the lineaments and digitizing the faults, all resulting structures were integrated using the ArcGIS Merge tool. This consolidated dataset was then utilized to create a fracture density map.

Lineament density

The importance of lineaments in landslide studies is fundamental. So, visible on satellite or aerial images, the lineaments reveal the deep architecture of the subsurface by delineating geological weakness zones such as faults and fractures. In risk assessment, these features can define potential planes of rupture and manage groundwater infiltration, which is a major landslide triggering factor. Therefore, in the present study; we used as a Landsat images, which is the preferred tool for mapping, and offers a synoptic view that identifies structures over large areas (Ramli et al., 2010). In the context of this study, lineament density-a key parameter used to quantify their prevalence within a given area-is defined as follows:

$$L_d = \frac{\sum_{i=1}^{n} L_i}{A} \quad (1)$$

where $\sum_{i=1}^{n} L_i$ represents the sum of individual lineament lengths [L], and A corresponds to the unit surface area of the study zone [L^2].

This metric helps evaluate the concentration of these structures and assists in identifying areas potentially more sensitive to tectonic movements. After extracting the lineaments from the Landsat 8 OLI/TIRS document, density map were generated using the "density" tool in spatial analysis, which calculates the lineament density around each raster cell.

Quantitative analysis of lineament density indicates that the maximum values are localized in the western High Atlas, a region characterized by a dense and intricate fault network. This elevated density shows a strong correlation with the area's main active tectonic structures, which are primarily governed by two major NE–SW trending faults – the Tizi n'Test fault and the south Atlas fault.

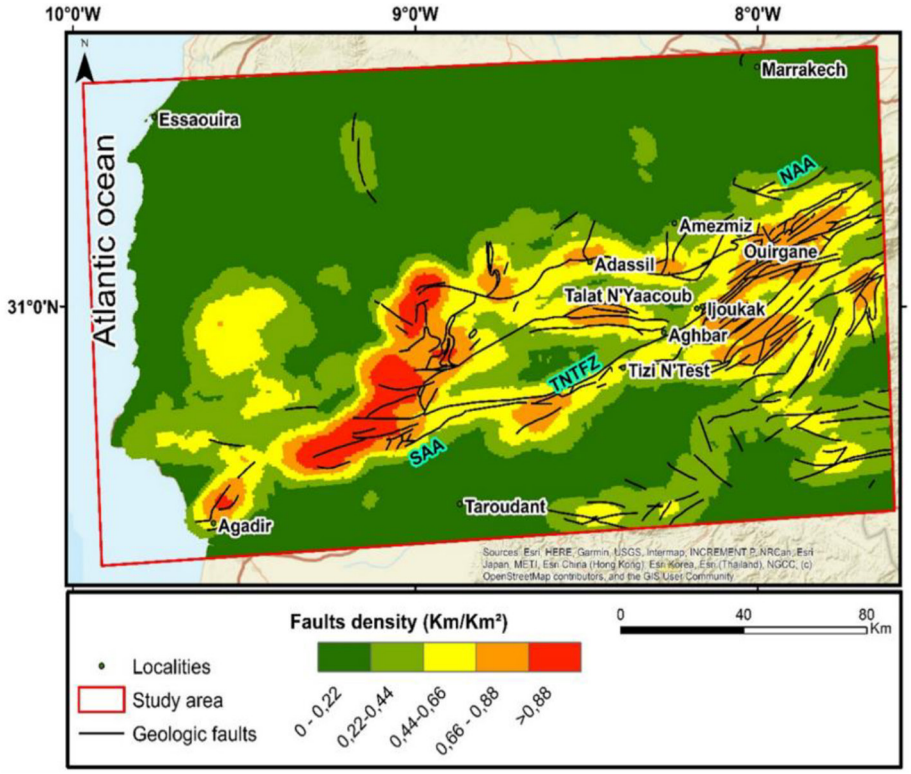

Figure 3. Map of lineaments density in the Moroccan High Atlas (TNTFZ – Tizi n'Test fault zone, SAA – South Atlasic Accident, NAA – North Atlasic Accident)

This specific orientation is consistent with the general axis of the mountain range and serves as a reflection of the regional tectonic stresses (Qarbous et al., 2003). Furthermore, the alignment of lineaments along this axis implies a recent reactivation of these deep crustal structures (Qarbous et al., 2025). The density map thus helps identify zones of active crustal deformation, overlaying the interpretation that the western High Atlas is a site of significant tectonic activity. The result map was categorized into five classes in km/km² (Figure 3): 0–0.22; 0.22–0.44; 0.44–0.66; 0.66–0.88; > 0.88

Lithology

Lithology is a fundamental analytical factor in landslide susceptibility modeling, influencing slope stability through key properties like strength, cohesion, and permeability (Mengistu et al., 2019). Landslides are often associated with rock strata characterized by low shear strength and reduced permeability (Sur et al., 2020). In this study's area, geological formations were categorized by their age, spanning from the Precambrian to the Quaternary. This classification was based on existing foundational documents after mentioned in geological faults section.

The oldest formations (Precambrian and Paleozoic), comprising schists, quartzites, and sandstones, mainly outcrop in the western Atlasic structures (Michard et al., 2008). The Mesozoic (detrital and carbonate series) forms the main High Atlas reliefs, structured during the Alpine orogeny in the Cenozoic (Frizon de Lamotte et al., 2008). Cenozoic deposits rest unconformably on the Mesozoic series (Tesón et al., 2010), while Quaternary formations (Ait Brahim et al., 2002) are located in valleys. This distribution establishes the structural framework, highlighting the susceptibility of marly formations and Quaternary cover deposits to instability (Guzzetti et al., 2012). The resulting map is divided into five age-based classes: Precambrian, Paleozoic, Mesozoic, Cenozoic, and Quaternary (Figure 4).

Seismic magnitudes

Earthquakes are a key triggering factor for landslides, particularly in regions with high seismic activity earthquake-generated vibrations lead to an immediate rise in pore-water pressure, which consequently reduces the shear strength of soils (Tanyas et al., 2017). This relationship is especially critical in mountainous areas, where

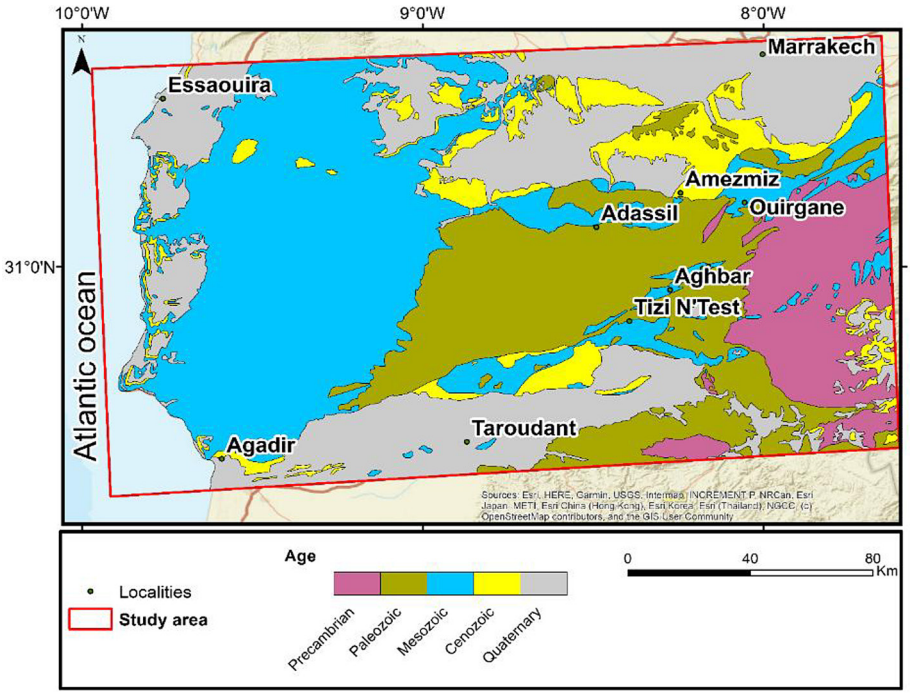

Figure 4. Map of lithology classes of the study area

the combination of steep slopes and seismic loading promotes slope failures. Analyses of major earthquakes demonstrate their ability to generate thousands of simultaneous landslides (Roback et al., 2018). In this study, the spatial distribution of seismic magnitudes in the western High Atlas was modeled in ArcGIS using the Spline interpolation method for seismic magnitudes, based on the seismic catalog of the National Geographic Institute (IGN: https://www.ign.es/web/en/ign/portal/sis-catalogo-terremotos) for the period 1910–2025. The analysis allowed the calculation of the residual magnitude anomaly (Z = Mobserved – Mmean), where Mobserved is the measured seismic magnitude and Mmean is the average seismic magnitude. This revealed a heterogeneous pattern with a corridor of high seismicity (magnitude > 4.0) between Agadir and Taroudant, coinciding with the south Atlas Fault. Positive anomalies (Z > 0) identify areas where the magnitude exceeds the regional mean, suggesting an accumulation of crustal stress, whereas negative anomalies (Z < 0) correspond to lower seismicity. The resulting map was classified into five intervals, establishing a direct correlation between these seismic anomalies and landslide susceptibility. This map, which is categorized into five classes (Figure 5), thus provides a valuable tool for integrated natural hazard assessment in the region.

Slope index

Slope, as a fundamental geomorphological parameter, is a predominant factor for slope stability. A detailed map of slope angles was created from the aforementioned 250-meter digital elevation model (DEM). The selected resolution offers an optimal compromise between vertical accuracy and regional-scale analysis, while maintaining a reasonable computational load for data processing (Wilson et al., 2007). The terrain was then classified into five distinct subclasses, illustrated in Figure 6. The analysis establishes a direct correlation between slope angle and susceptibility to instability. Steep slopes, characterized by high gradients, exhibit a significantly greater predisposition to landslides than moderate to gentle slopes. According to soil mechanics, this causal relationship is explained by the fact that the steepness of a slope generates greater shear stresses, increasing the probability of failure (Achour et al., 2017). Conversely, low-angle slopes, associated with negligible shear loads due to their gentle gradient, offer considerably more stable conditions and a lower probability of triggering mass movements (Ajin et al., 2016). Thus, the slope gradient is confirmed as the determining factor for assessing landslides hazard in this type of study. The resulting map is categorized into five classes (Figure 6).

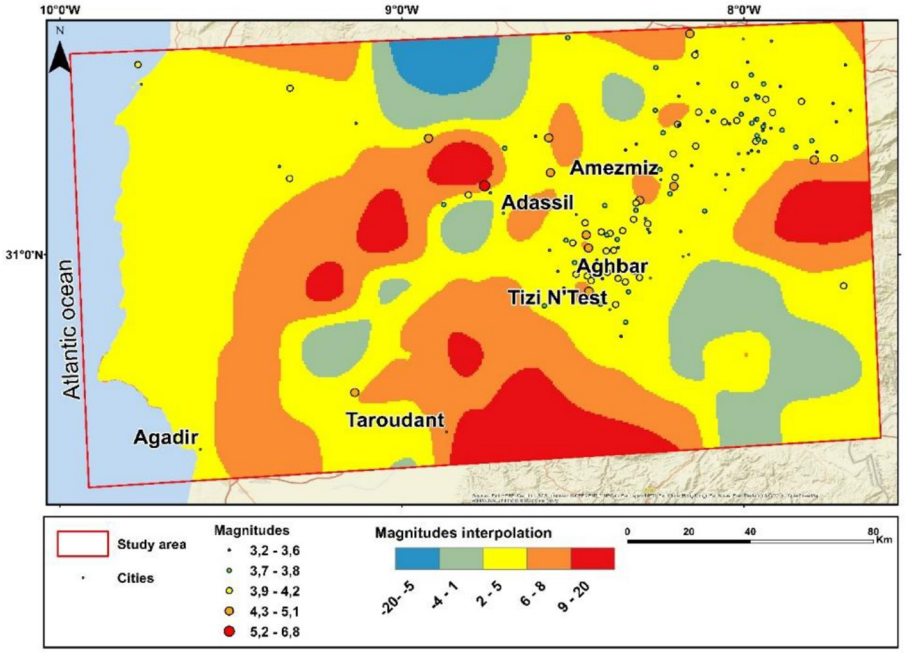

Figure 5. Magnitude interpolations for the study area between 1910 and 2025, provided by the Spanish National Geographic Institute (IGN)

Aspect

Defined by the orientation of slopes regarding sunlight and prevailing winds, Aspect functions as an indirect factor affecting the occurrence of landslides (Das et al., 2022). The aspect map was created from the SRTM DEM, previously used for the morpho-structural analysis. It was computed in ArcGIS 10.8 using the "aspect" tool, which determined the slope orientation for each pixel on an angular scale from 0° to 360°. The resulting directions were then reclassified into eight principal classes (Figure 7): north, northeast, east, southeast, south, southwest, west, and northwest. This mapping aims to characterize the organization of slopes and identify the dominant structural directions in the western High Atlas. Statistical and visual

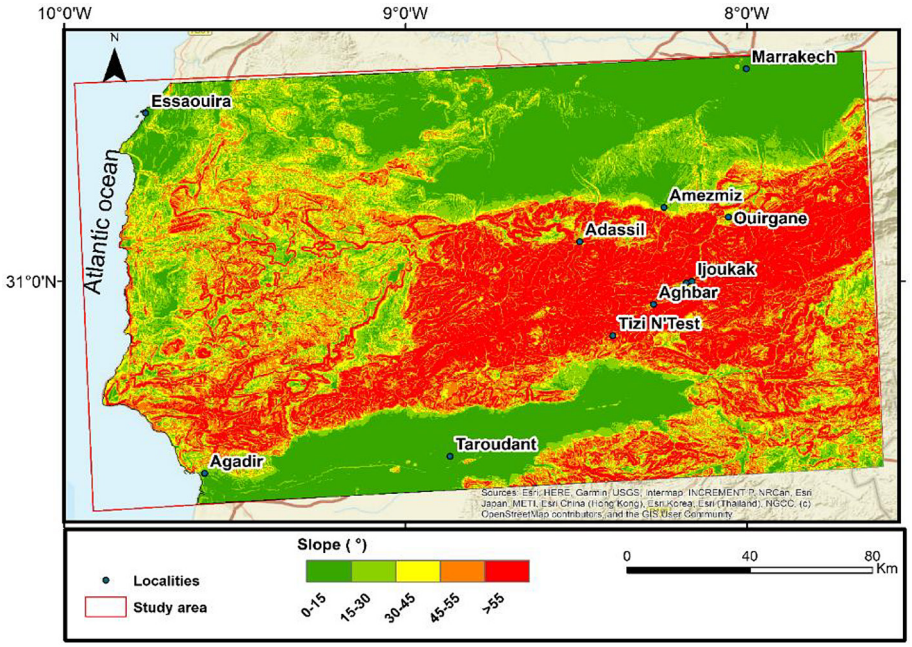

Figure 6. Map of slope classes

analysis of these orientations provides major insights into the tectonic controls shaping the landscape and helps to cross-validate the fracture and lineament networks identified in previous steps (Masoud and Koike, 2011). The most common slope directions (NE–SW and E–W) coincide with the major tectonic structures of the region, such as the deformation corridor of the Tizi n'Test fault (Ait Brahim, 1991; Morel et al., 2000). The resulting map is categorized into eight classes (Figure 7)

Curvature profile

Curvature, represents the second derivative of a surface. A positive value denotes a convex surface, a negative value indicates a concave surface, and a zero value signifies a flat surface. In the assessment of landslide susceptibility, this parameter functions as an indirect indicator of effects related to water (Ohlmacher, 2007). Curvature, as a factor, reflects water's indirect influence on the zonation of landslide hazards. Convex or concave slopes are prone to retaining more water for a longer duration following intense rainfall (Chen et al., 2017). The terrain curvature map was generated from the previously mentioned DEM using the "curvature" tool in ArcGIS 10.8. To correct the unit discrepancy between the planimetric coordinates (degrees) and elevation values (meters) and thus ensure metric accuracy in morphometric calculations, a Z-factor of 0.00001036 was applied for the study area. The current study area (Figure 8) exhibits a combination of flat, concave, and convex curvatures.

Hydrographic network density

The degree of development of the drainage network is an essential geomorphological metric, as it quantifies the spatial organization of flow channels (Subedi et al., 2023). A high drainage density intensifies soil degradation through erosion, reduces ground bearing capacity, and increases landslide hazard (Bahrami et al., 2020; Panchal et al., 2022). The modeling of this variable was based on the digitization of the basin's hydrographic network, combined with topographic data from the previously used DEM, ensuring topographic consistency across all datasets of the study. Processing was carried out in ArcGIS by sequentially applying the fill, flow direction, and flow accumulation tools to model surface runoff. A thresholding step was then performed using the conditional tool on the flow accumulation layer, retaining only values greater than 1000 to extract permanent and significant hydrographic segments (Tarboton et al., 1991). A systematic organization in the drainage density of the western High Atlas is

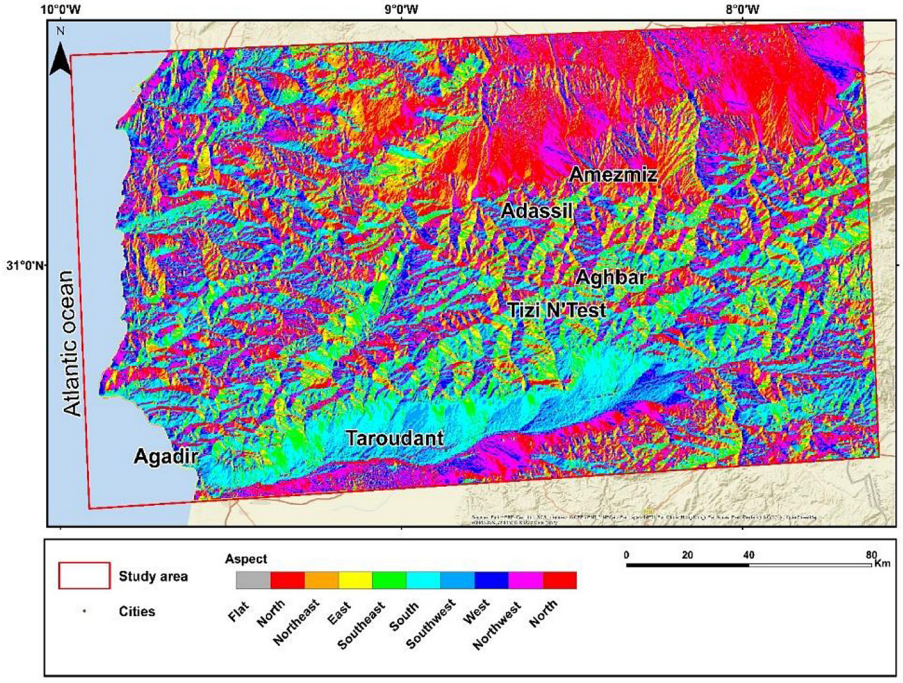

Figure 7. Map of aspect

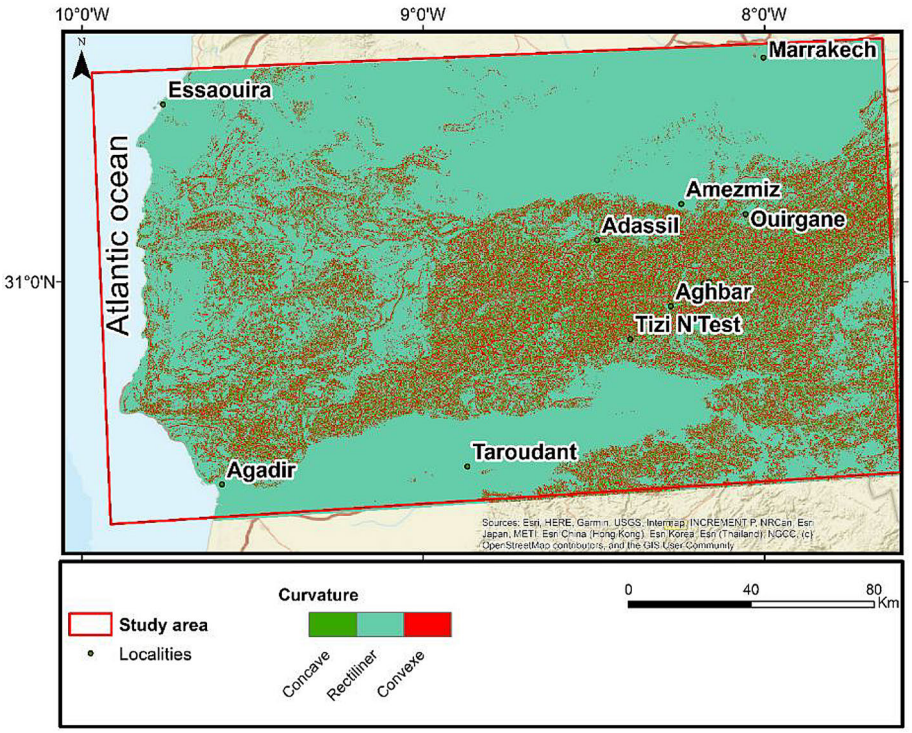

Figure 8. Map of profile curvature

evident, controlled primarily by the geological structure and tectonic uplift. Strong structural control is clearly demonstrated by the network's dendritic to rectangular architecture, especially in the cental massif of the western High Atlas, and the alignment of streams parallel to major faults like the Tizi n'Test fault (Ait Brahim, 1991; Keller and Pinter, 2002). The final map is divided into five categories (Figure 9).

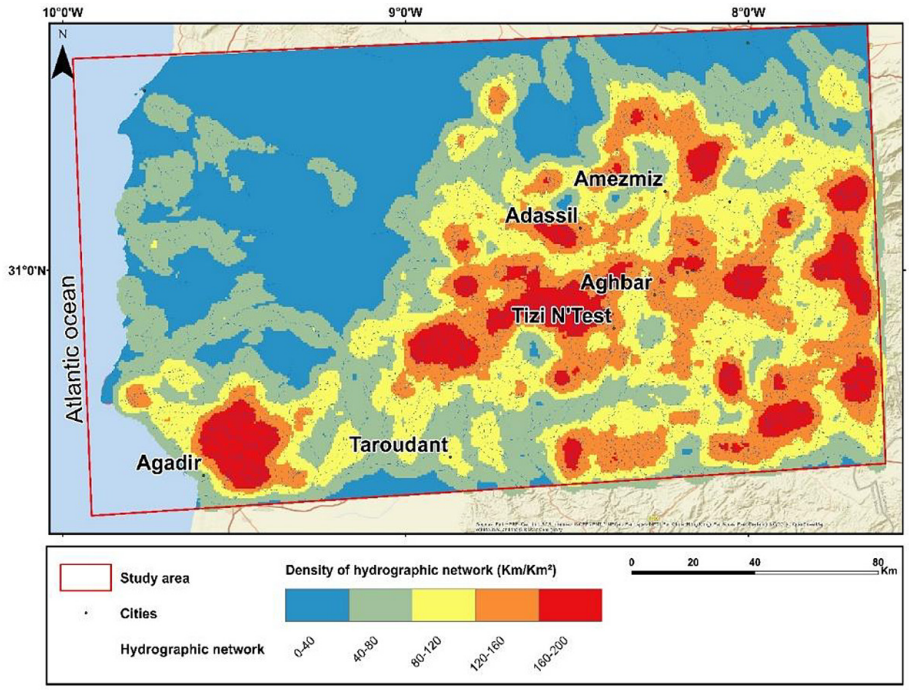

Figure 9. Map of the hydrographic network density classes

The analytic hierarchy process – weighted sum method

The AHP is a widely adopted semi-quantitative approach frequently employed in the development of landslide susceptibility maps. Its primary purpose is to assess and compare the potential contribution of various information layers to the occurrence of these phenomena. AHP is designed to structure complex decision-making processes by systematically integrating expert judgment (Saaty and Vargas, 1980). Specifically, the method determines the relative weight of each factor involved in evaluating conditions that favor landslides. The procedure begins by identifying the thematic layers that influence susceptibility. In this study, we utilized: slope, aspect, curvature, faults and lineaments, hydrographic network, interpolation of seismic magnitudes, and lithology. The relevance of these components to landslide occurrence in a given area depends on the probable impact of each parameter; consequently, each factor is assigned a specific weight. The combined effect of all these factors ultimately leads to a reliable susceptibility model. The foundation of the AHP method is the pairwise comparison matrix. Within this matrix, every factor is systematically compared to every other factor based on its perceived influence on landslide susceptibility. This comparison utilizes a rating scale from 1 to 9: a value of "1" indicates equal importance between the two factors, whereas a value of "9" signifies that one factor is absolutely dominant. The matrix thus synthesizes the weights assigned by the expert, reflecting the relative importance of each criterion (Saaty and Vargas, 1980). In this case, we applied the AHP method in three successive steps to evaluate landslide susceptibility: building a pairwise comparison matrix for each landslide-triggering factor; calculating the weight of each factor; validating the consistency of the results based on the consistency ratio (CR) (Saaty and Vargas, 1980). In summary, these weights indicate that the factors contribute to different degrees according to their impact on landslide susceptibility. For instance, if the calculated weight of magnitude is 0.35, this means it represents 35% of the importance in the final decision. The consistency ratio is expressed as:

$$CR = CI / RI \tag{2}$$

where: CI – represents the consistency index and corresponds to the degree of deviation from consistency, and RI – the random index corresponds to a standard index derived from randomly constructed matrices of the same size).

A CR value below 0.1 is typically considered acceptable, which signifies that the comparisons made are consistent (i.e., CR < 0.1) (Saaty, 1980). In the present analysis, the calculated CR is 0.024 (Figure 10).

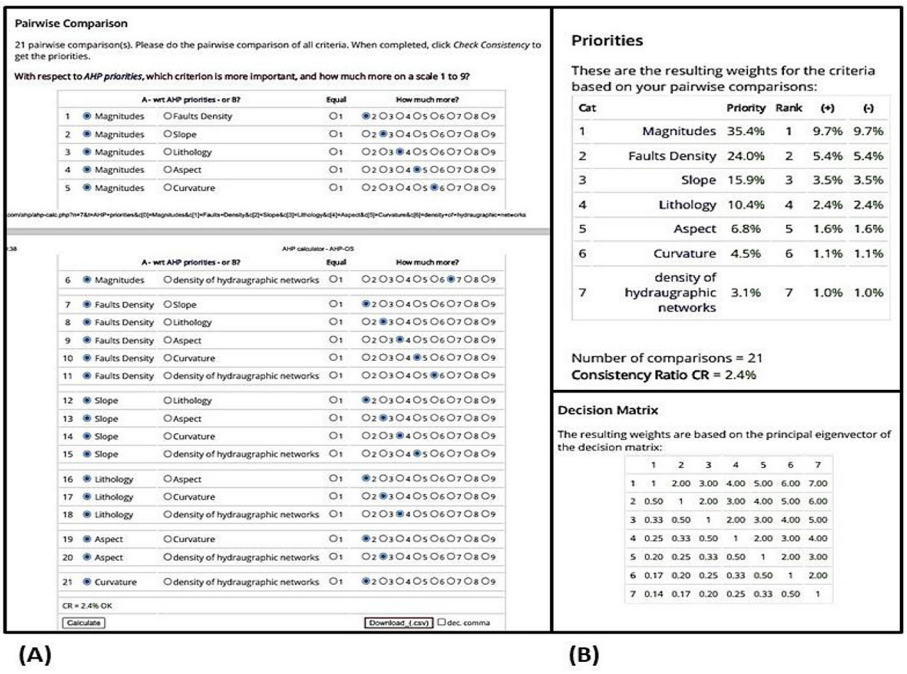

Figure 10. (A & B) AHP implementation

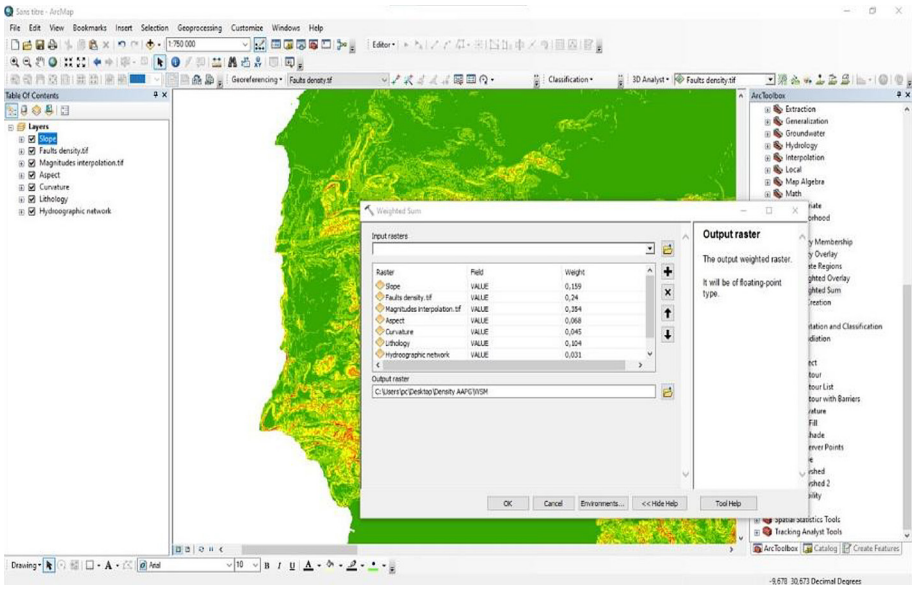

Figure 11. Weighted sum method

After calculating the weights, the susceptibility map was created in ArcMap using the weighted sum method (WSM). The fundamental principle of this approach involves aggregating the relative weighting of multiple sets of conditioning variables. For landslide susceptibility mapping, two levels of weighting were applied: (i) assigning a relative weight to the classes of each variable, reflecting their estimated importance in the landslide process; (ii) weighting the predictors themselves via the pairwise comparison method. After normalizing the criterion scores and calculating the weights, the susceptibility index map was generated using the weighted sum model (WSM). This method, which is commonly employed to solve one-dimensional problems, integrates the different criteria into a single evaluation score. According to the WSM, each criterion's score is multiplied by its respective weight. The overall susceptibility index is then obtained by summing these weighted criteria, as formalized in the following equation (Fishburn, 1967):

$$A^{WSM} = \sum_i^n (X_a\, Y_b) \tag{3}$$

where: a – represents the factor; X – corresponds to the weight assigned to the factor; b – represents the classes of the factor; Y – corresponds to the rank of the factor's subclasses.

The determination of weights is critical to the aggregate score. Given that the factor weights accumulate additively, the final scores generated on the map are expressed on a normalized scale. Furthermore, the weights assigned to each criterion define its relative importance compared to the other explanatory factors (Figure 11).

MODEL AND DATA VALIDATION

Empirical model

The mapping of landslide susceptibility for the Western High Atlas was performed using ArcGIS geomatics tools. The foundation for this approach rested on the results yielded by the AHP method. The procedure entailed aggregating the responsible factors and their weighting coefficients (influence weights) to produce a map (Figure 12) that delineates the varying degrees of risk susceptibility. This risk is categorized into five levels spanning the entire area: very low, low, moderate, high, and very high. The establishment of these susceptibility classes is directly associated with the presence of the parameters deemed most determinative for terrain instability. Cartographic analysis (geological maps and satellite images) facilitated the categorization of five major classes of landslides (Figure 12). This distinction was based on seven parameters such as lithology, faults density, magnitudes interpolation, aspect, curvature, hydrographic networks and slope. Following a qualitative analysis and the application of the AHP to the identified factors, a landslide susceptibility map was generated. The

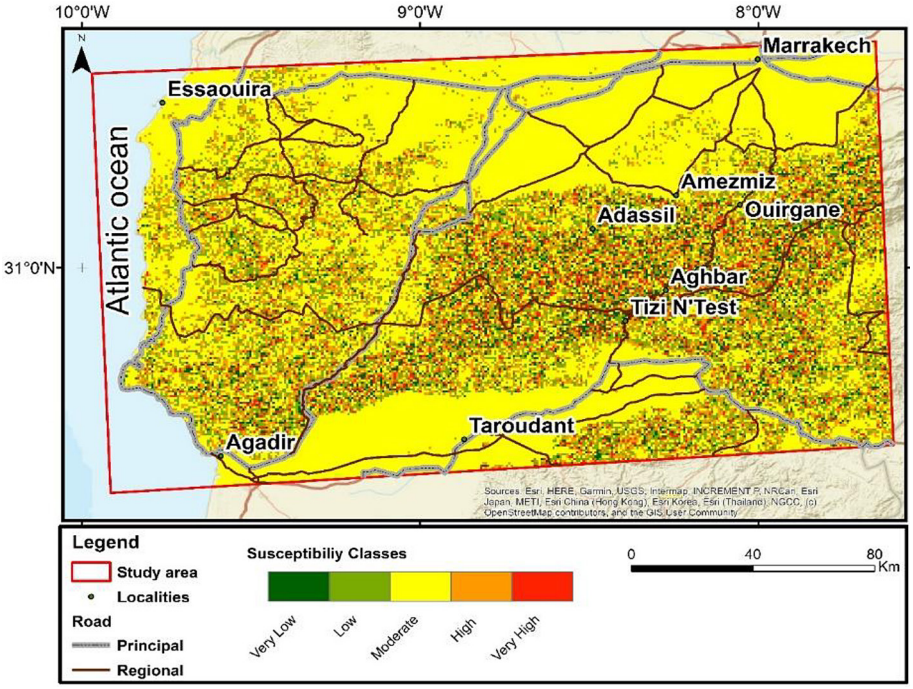

Figure 12. Landslide susceptibility map in the Western High Atlas

succeeding section of the research analyzes the contribution of individual factors and gauges the map's dependability. The model obtained (Figure 12; Table 2) reveals that 5.30% of the total area (32 123,1 km²) corresponds to the zone of the very high landslide susceptibility, 15.10% high susceptibility, 59.41% moderate susceptibility, 14.91% and 5.27% low to very low susceptibility. The total area of moderate to very high susceptibility represents approximately 72.24% of the total area (32 123,1 km²), indicating that the risk is very important in the region.

Data validation

To identify areas susceptible to landslides triggered by the Al Haouz earthquake, we used the Preferred Landslide Model of Jessee et al. 2018 from the USGS database, available at website.

Table 2. The percentages of landslide susceptibility classes

Susceptibility classes	Count	Percentage
Very Low	3002	5,27
Low	8487	14,91
Moderate	33820	59,41
High	8594	15,10
Very high	3019	5,30

The model was developed immediately after the Al Haouz seismic event to visualize the affected areas. An inventory of 158 points was created by examining areas prone to landslides, focusing on the High Atlas Massif where steep slopes, mountainous regions, and cliffs are prominent. We identified indicators of rockfalls on Field trip, which confirm the presence of landslides, as well as the accumulation of debris on the roads of Imi n'Tala and Ijoukak. The correlation between areas affected by landslides from the Preferred Landslide Model and the susceptibility classes of our model indicate that the high and very high susceptibility categories corresponds to the majority of movements already identified in the region (notably at Imi n'Tala, Tahnaout, Azegour, Oued n'Fiss, Ijoukak). We detected that 41 points are in the very high class, 30 points in the high class, 43 points in the moderate class, 24 points in the low class, and 18 points in the very low class (Figure 12 and 13). The affected areas were documented using landmarks on the USGS model for identification purposes. The data were recorded and exported to create a GIS database for subsequent analyses and interpretations. This study demonstrates that landslides triggered by the El Haouz earthquake are predominantly concentrated in regions characterized by a medium to high density of tectonic faults and on steep slopes, thereby represent a close relationship between geological structures, ground

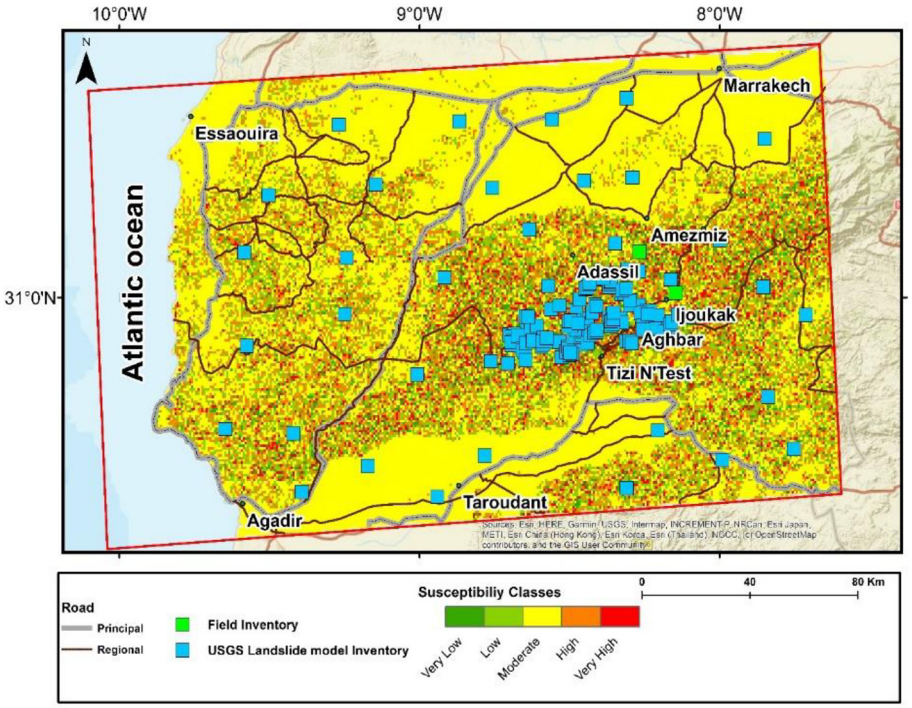

Figure 13. Landslide susceptibility map of western High Atlas

topography and landslide susceptibility. Throughout the seismic event, rockfalls were observed to initiate at the summit of ridges, underscoring the significance of local topography in such geological contexts. The affected areas are primarily constituted of highly deformed Precambrian and Paleozoic crystalline schists, succeeded by Cenozoic deposits (continental Miocene) and culminating in Mesozoic rocks (from the Triassic to the Cretaceous). Landslides in Quaternary plains, notably in the El Haouz plain, are generally moderate in intensity. The combination of lithological fragility

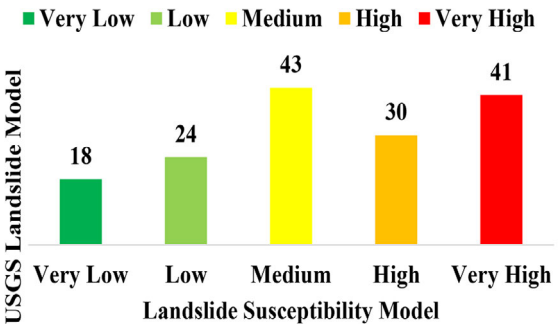

Figure 14. Comparison of landslide susceptibility classes based on the USGS landslide model

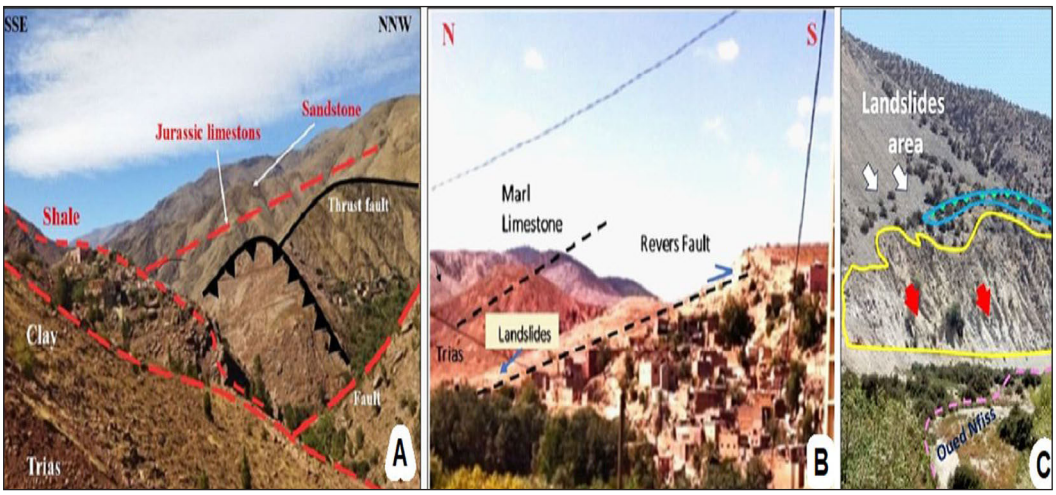

Figure 15. Landslides in the region: (A) Tahnaout, (B) Azegour, (C) Oued n'Fis

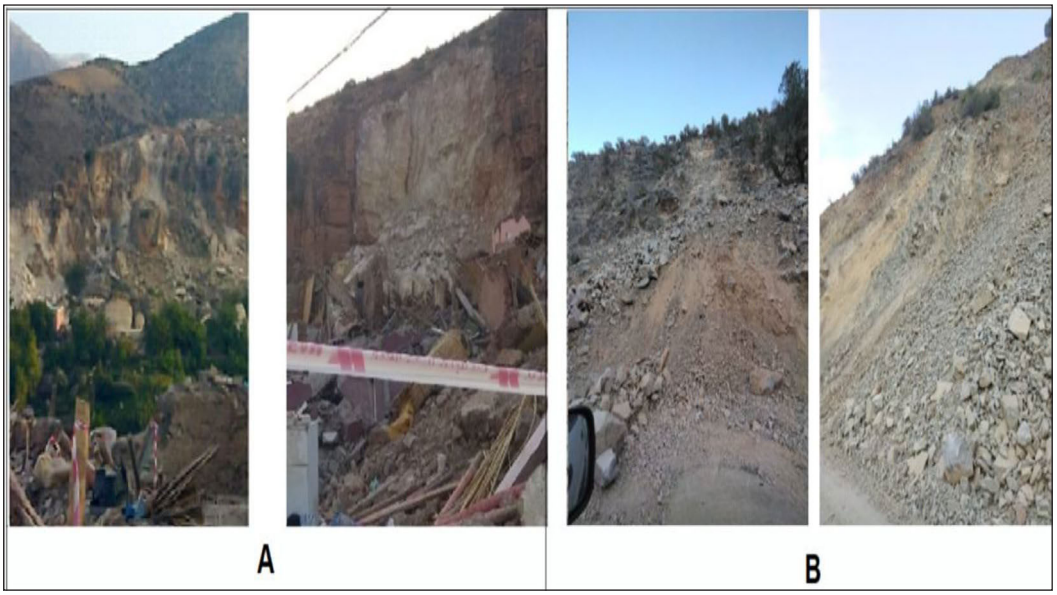

Figure 16. Photo of landslides in the: (A) Imi n'Tala area, (B) Ijoukak area

with the effects of mechanical and chemical weathering has been demonstrated to increase the risk of rockfalls during earthquakes (Labriki et al., 2025). It is therefore essential to take geological, lithological and topographical factors into account when assessing landslide risks and implementing risk management measures in areas of high seismic activity. The inventory and field investigations corroborate the results shown on the landslide susceptibility map for the study area. The USGS model and satellite imagery, particularly those captured following the Al Haouz earthquake, enabled the identification of several landslide-prone areas that are consistent with those already delineated on the generated map. This study sector presents a significant challenge, as the majority of zones impacted by this phenomenon are situated within residential areas (Figures 13–16).

CONCLUSIONS

The analytic hierarchy process, weighted sum method was employed to generate a landslide susceptibility map for the Al Haouz region. The analysis identified several key factors influencing landslides, including seismic magnitudes, faults, aspect, slope, curvature, lithology, and the hydrographic network. In the affected area, the results show that topography and seismic activity are the main predisposing factors, while seismic foci, their magnitudes, and faults act as the primary triggers. The five-class susceptibility map, synthesized from these factors, highlights the central High Atlas massif, specifically the Imi n'Tala, Tahnaout, Azegour and Ijoukak areas, as particularly vulnerable sectors. These zones require increased vigilance during the construction of infrastructures such as homes and dams. In conclusion, the susceptibility map developed in this study, constitutes a fundamental tool for territorial planning and risk management in the Al Haouz region, particularly in the post-seismic context. The results of this research are also applicable as a foundation for geological and prevention studies in analogous environments.

REFERENCES

1. Abdallah, M., Shahrour, I., Hage Chehade, F. (2013). Analyse du comportement sismique des massifs rocheux inclinés fracturés – Application au massif de Jezzine – Liban, *21ème Congrès Français de Mécanique*,1–6.
2. Achour, Y., Boumezbeur, A., Hadji, R., Chouabbi, A., Cavaleiro, V., Bendaoud, E.A., (2017). Landslide susceptibility mapping using analytic hierarchy process and information value methods along a highway road section in Constantine, Algeria. *Arabian J. Geosci. 10.* https://doi.org/10.1007/s12517-017-2980-6
3. Ajin, R.S., Loghin, A.M., Vinod, P.G., Jacob, M.K., Krishnamurthy, R.R., (2016). Landslide susceptible zone mapping using ARS and GIS techniques in selected taluks of Kottayam district, Kerala, India. *Int J Appl Remote Sens GIS 3*(1), 16–25.
4. Ait Brahim, L. (1991). *Tectonique cassante et*

états de contraintes récents du Maroc: Apport à l'évaluation de l'aléa sismique. Thèse de Doctorat d'Etat, Université Mohammed V, Rabat. 360.

5. Amaya, A., Algouti, Ab., Algouti, Ah., El Aaggad, N., (2014). Cartographie de l'aléa mouvements de terrain du bassin versant de N'fis, Haut Atlas, Maroc, *International Journal of Innovation and Applied Studies, 8*(2), 645–652. https://doi.org/10.14195/978-989-96253-3-4_30
6. Amrhar, M. (2002). Paléocontraintes et déformations syn-et post-col lision Afrique–Europe identifiées dans la couverture mésozoïque et cénozoïque du Haut Atlas occidental (Maroc), C.R. *Geosci. 334*(4), 279–285. https://doi.org/10.1016/s1631-0713(02)01730-3
7. Ambroggi, R. (1963). Etude géologique du versant méridional du Haut Atlas occidental et de la plaine du Souss 1/50 0000, *Notes & Mém. Serv. Géol. Maroc*, *157*, 322.
8. Asebriy, L., Cherkaoui, T.E., (1995). Tectonique cassante et sismotectonique dans le Rif et son avant-pays (Maroc), *Africa Geoscience Review, 2*(1), 141–149. https://doi.org/10.1016/0899-5362(93)90023-j
9. Azzouz O., El Fellah B., Chalouan, A. (2002). Processus de glissement dans le Massif de Bokoya (Rif interne, Maroc): exemple de Cala Bonita. *Bulletin Institut scientifique., Section Sciences de la Terre, 24,* 33–40.
10. Bahrami, S., Rahimzadeh, B., Khaleghi, S. (2020). Analyzing the effects of tectonic and lithology on the occurrence of landslide along Zagros ophiolitic suture: a case study of Sarv-Abad, Kurdistan, Iran. *Bulletin of Engineering Geology and the Environment, 79*(3), 1619–1637.
11. Bao, M., Abdelaal, M. I., Saleh, M., Chourak, M., Mohamed, M., Xing, M., (2025). Unlocking the hidden secrets of the 2023 Al Haouz earthquake: Coseismic model reveals intraplate reverse faulting in Morocco derived from SAR and seismic data, International *Journal of Applied Earth Observation and Geoinformation, 137*, 104420, 1–15, https://doi.org/10.1016/j.jag.2025.104420
12. Baudon, C., Fabuel-Perez, I., Redfern, J., (2009). Structural style and evolution of a Late Triassic rift basin in the Central High Atlas, Morocco: controls on sediment deposition. Geological Journal Special Issue 44(6), 677–691. https://doi.org/10.1002/gj.1195
13. Beauchamp, W., Barazangi, M., Deminati, A., El Algi, M., (1996). Intracontinental rifting and inversion: Missour Basin and Atlas Mountains, Morocco. American Association of Petroleum Geologists Bulletin 80, 1459 – 1482. https://doi.org/10.1306/64ed9a60-1724-11d7-8645000102c1865d
14. Brede, R., Hauptmann, M., Herbig, H.-G. (1992). Plate tectonics and intracratonic mountain ranges in Morocco-The Mesozoic-Cenozoic development of the Central High Atlas and the Middle Atlas. *Geol. Rundsch. 81*, 127–141, https://doi.org/10.1007/bf01764544
15. Blackburn, T. J., Olsen, P. E., Bowring, S. A., McLean, N. M., Kent, D. V., Puffer, J., McHone, G., Rasbury, E. T., Et-Touhami, M. (2013). Zircon U-Pb geochronology links the end-triassic extinction with the central Atlantic magmatic province. Science, 340(6135), 941–945. https://doi.org/10.1126/science.1234204
16. Chen, W., Xie, X., Wang, J., (2017). A comparative study of the logistic model tree, random forest, and classification and regression tree models for spatial prediction of landslide susceptibility. *Catena 151*, 147–160.
17. Cherkaoui T.-E, El Hassani A. (2015). Evaluation et atténuation de l'aléa sismique au Maroc. Actes de la session plénière solennelle, 24–26 février 2015, *Académie Hassan II des sciences et techniques, Rabat*, 157–173.
18. Cherkaoui T.-E., El Hassani A., Azaoum M. (2017). Impacts du tremblement de terre de 1755 au Maroc : histoire, société et religion. In Witnesses of Chaos: aspects of the 1755 Lisbon earthquake, *Academia das Ciências de Lisboa*, 53–68.
19. Choubert, G., (1971). Carte géologique du Maroc, Feuille de Tarhazoute au 1/100 000, *Edition du Service Géologique du Maroc, Notes et Mémoires N° 204.*
20. Das, S., Sarkar, S., Kanungo, D.P., (2022). GIS-based landslide susceptibility zonation mapping using the analytic hierarchy process (AHP) method in parts of Kalimpong Region of Darjeeling Himalaya. *Environ. Monit. Assess. 194*, 1–28.
21. Dutour, A., Ferrandini, J. (1985). Nouvelles observations néotectoniques dans le Haut Atlas de Marrakech et le Haouz central (Maroc). Apports sur l'évolution récente d'un segment du bâti atlasique. *Revue de géologie dynamique et de géographie physique, 26*(5), 285–297.
22. Domènech, M., A. Teixell, J. Babault, and M.-L. Arboleya. (2015). The inverted Triassic rift of the Marrakech High Atlas: A reappraisal of basin geometries and faulting histories, *Tectonophysics 663*, 177–191, https://doi.org/10.1016/j.tecto.2015.03.017 El Arabi E.H., Ferrandini J., Essamoud R. (2003). Triassic stratigraphy and structural evolution of a rift basin: the Eç-Çour basin, High Atlas of Marrakech, Morocco. *J. Afr. Earth Sci. 36*, 29–39. https://doi.org/10.1016/s0899-5362(03)00020-4
23. El Aaggad. Algouti, Ah, Algouti Ab., Lahbani I., Amaya A. (2014). Risque mouvements de terrain sur le versant sud du Haut Atlas Central: cas du bassin versant du Dades, *Colloque International sur les utilisateurs des SIG GIS, Meknès.*
24. El Fellah, B., Azzouz, O., Asebriy, L. (1996). Sikha Asfalou: exemple de glissement sur la côte méditerranéenne des Bokoya entre Torrès et Badis, (Rif septentrional, Maroc). *Bulletin-Réseau Erosion, 16*, 222–231.

25. EL Qayedy, J., Taj-Eddine, K., Bonn, F., Chikhaoui, M., Witam, O. (2006). Caractérisation lithologique du Haut Atlas marocain à l'aide des données ASTER et des mesures spectrales de terrain. Télédétection, *Revue Française de Photogrammétrie et de Télédétection, 6*(2), 153–175.
26. Ennassiri, B. Mouak, S. (2021). Vulnérabilité aux aléas sismiques dans la ville d'Agadir–Maroc. Etude par systèmes d'information géographique. *Annalele Universitii Bucaresti, Geografie,* 15–31. https://doi.org/10.5719/aub-g/70.1/3
27. Fekkak, A., Ouanaimi, H., Michard, A., Soulaimani, A., Ettachfini, E.M., Berrada, I., El Arabi, H., Lagnaoui, A., Saddiqi, O. (2018). Thick-skinned tectonics in a Late Cretaceous-Neogene intracontinental belt (High Atlas Mountains, Morocco): The flat-ramp fault control on basement shortening and cover folding, *Journal of African Earth Sciences, 140,* 169–188. https://doi.org/10.1016/j.jafrearsci.2018.01.008
28. Fraissinet, C., Zouine, E.M, Morel, J.L, Poisson, A., Andrieux, J., Faure-Muret, A. (1988). Structural evolution of the southern and Northen Central High Atlas in Palaeogene and Moi-Pliocene times. In Jacobshagen, V. (Ed). The Atlas System of Morocco : Studies on its Geodynamic Evolution, *Springer-Verlag, Berlin,* 273–291. https://doi.org/10.1007/bfb0011597
29. Fishburn, P.C., (1967). Letter to the Editor—Additive Utilities with Incomplete Product Sets: Application to Priorities and Assignments. *Operations Research 15*(3), 537–542. https://doi.org/10.1287/opre.15.3.537
30. Frizon de Lamotte, D., Zizi, M., Missenard, Y., Hafid, M., El Azzouzi, M., Maury, R.C., Charriere, A., Taki, Z., Benammi, M., and Michard, A.(2008). The Atlas System. In Continental Evolution: The Geology of Morocco 133–202. *Springer, Berlin, Heidelberg.* https://doi.org/10.1007/978-3-540-77076-3_4
31. Froitzheim, N. (1988). Sedimentary and synorogenic normal faults within a thrust sheet of Eastern Alps (Ortler zone, Graubunden, Switezeland) : *Eclogae Geologicae Helvetiae, 81*, 593–610.
32. Geological Map of Morocco, Scale :1/1000 000, *Editions du Service géologique, Notes et mémoires, N°260, Publiée en 1985.*
33. Ghorbal, B., Bertotti, G., Foeken, J., Andriessen, P. (2008). Unexpected Jurassic to Neogene vertical movements in stable parts of NW Africa revealed by low temperature geochronology. *Terra Nova, 20*(5), 355–363. https://doi.org/10.1111/j.1365-3121.2008.00828.x
34. Guzzetti, F., Mondini, A. C., Cardinali, M., Fiorucci, F., Santangelo, M., Chang, K. T. (2012). Landslide inventory maps: New tools for an old problem. *Earth-Science Reviews, 112*(1–2), 42–66. https://doi.org/10.1016/j.earscirev.2012.02.001
35. Havenith, H.-B., Bourdeau, C. (2010). Earthquake induced hazards in mountain regions: A review of case histories from Central Asia. *Geologica Belgica, 13,* 135–150.
36. Ibouh, H., and D. Chafiki (2017). La tectonique de l'Atlas: âge et modalités, *Géologues 194*, 24–28.
37. Jenny, J. (1983). Les décrochements de l'Atlas de Demnat (Haut Atlas central, Maroc): Prolongation orientale de la zone de décrochement du Tizi-n-Test et clef de la compréhension de la tectonique atlas ique, *Eclogae Geol. Helv. 76*(1), 243–251.
38. Keefer, D. K. (1984). Landslides caused by earthquakes. Geological Society of America Bulletin, 95(4), 406-421.
39. Keller, E. A., Pinter, N. (2002). Active Tectonics: Earthquakes, Uplift, and Landscape (2nd ed.). *Prentice Hall.*
40. Labriki, A., Bouchatta, Y., Labriki, K., Hassani, A., Zoraa, S., Chakiri, S., Ghazi, A. (2025). Co-seismic landslide mapping following the 2023 El Haouz earthquake using differential interferometric synthetic aperture radar and optical imagery (High Atlas, Morocco), *Ecological Engineering & Environmental Technology, 26*(8), 57–72. https://doi.org/10.12912/27197050/207169
41. Laville, E., Piqué, A., (1991). La distension crustale atlantique et atlasique au Maroc au début du Mésozoïque: le rejeu des structures hercyniennes. *Bulletin de la Société´ Géologique de France 162,* 1161–1171.
42. Levandowski, W. (2023). Fault-Slip Potential near the Deadly 8 September 2023 Mw 6.8 Al Haouz, Morocco, Earthquake, *The Seismic Record. 3*(4), 367–375, https://doi.org/10.1785/0320230037
43. Liu, X., Shao, S., & Shao, S. (2024). Landslide susceptibility zonation using the analytical hierarchy process (AHP) in the Great Xi'an Region, China. Scientific reports, 14(1), 2941. https://doi.org/10.1038/s41598-024-53630-y
44. Makkaoui, M., Azzouz, O., Tendero-Salmeron, V., Belhadj, K., Galindo-Zaldivar, J. (2024). The neotectonic deformation of the Eastern Rif Foreland (Morocco): New insights from morphostructural analysis. *Appl. Sci., 14,* 4134. https://doi.org/10.3390/app14104134
45. Masoud, A., Koike, K. (2011). Auto-detection and integration of tectonically significant lineaments from SRTM DEM and remotely-sensed geophysical data. ISPRS *Journal of Photogrammetry and Remote Sensing, 66*(6), 818–832. https://doi.org/10.1016/j.isprsjprs.2011.08.003
46. Mattauer, M., Proust, F. and Tapponier, P. (1972). Major strike slip-fault of late Hercynian age in Morocco. *Nature 237,* 5351, 160–162. https://doi.org/10.1038/237160b0
47. Mattauer, M., P. Tapponnier, and F. Proust (1977). Sur les mécanismes de formation des chaines

intracontinentales; l'exem ple des chaines atlasiques du Maroc, *Bull. Soc. Géol. Fr. 7*(3), 521–526, *https://doi.org/10.2113/gssgfbull.s7-xix.3.521*

48. Medina, F. (1994). Evolution structurale du Haut-Atlas Occidental et des régions voisines du Trias a l'actuel. Dans le cadre de l'ouverture de l'Atlantique central et la collision Afrique–Europe. *Unpublished State Doctorate (Doctorat de 3ème Cycle), Univ. Mohammed V, Rabat/ Morocco, 271.*
49. Medina, F., Errami, A. (1996). L'inversion tectonique dans le bassin triasique de Tine Melil (Haut atlas occidental, Maroc). *Implications sur le fonctionnement de la faille de Tizi n'Test. Gaia, 12,* 9–18.
50. Mengistu, F., Suryabhagavan, K.V., Raghuvanshi, T.K., Lewi, E., (2019). Landslide hazard zonation and slope instability assessment using optical and InSAR data: a case study from Gidole town and its surrounding areas, Southern Ethiopia. *Remote Sens Land 3*(1), 1–14. https://doi.org/10.21523/gcj1.19030101
51. Michard, A., Soulaimani, A., Hoepffner, C., Ouanaimi, H., Baidder, L., Rjimati, E. C., Saddiqi, O. (2008). The Variscan Belt. In Continental Evolution: The Geology of Morocco 65–132. *Springer, Berlin, Heidelberg.* https://doi.org/10.1016/j.tecto.2010.05.021
52. Michard, A., Soulaimani, A., Hoepffner, C., Ouanaimi, H., Baidder, L., Rjimati, E.C., Saddiqi, O. (2010). The South-Western Branch of the Variscan Belt : evidence from Morocco. *Tectonophysics, 492,* 1–24. https://doi.org/10.1016/j.tecto.2010.05.021
53. Morel, J. L., Meghraoui, M., Dahmani, M. (2000). Active faulting and seismicity in the Moroccan Atlas. *Journal of African Earth Sciences, 30*(1), 85–94. https://doi.org/10.1016/s0899-5362(00)00051-8
54. Morel, J.-L., E.-M. Zouine, J. Andrieux, and A. Faure-Muret (2000). Déformations néogènes et quaternaires de la bordure nord haut atlasique (Maroc): Rôle du socle et conséquences structurales, *J. Afr. Earth. Sci. 30*(1), 119–131, https://doi.org/10.1016/s0899-5362(00) 00011-7
55. Moore, G.K. (1983). Objective procedures for lineamant enhancement and extraction, *n5, Photogramm. Eng. Rem. Sens. 49*, 641–647.
56. Nouayti, A., El Moudnib, L., Khattach, D., Zeckra, M., Nouayti, N., Saadi, O., El Hairechi, K., Oujane, B., Iken, H. (2024). Seismic synthesis of the Al Haouz earthquake of September 8th, 2023 by integrating gravimetric and aeromagnetic data from the western High Atlas in Morocco, *Model. Earth Syst. Environ.,* 1–20, https://doi.org/10.1007/s40808-024-02148-3
57. Ohlmacher, G. C. (2007). Plan curvature and landslide probability in regions dominated by earth flows and earth slides. *Engineering Geology, 91*(2–4), 117–134.
58. Olsen, P.E., Kent, V.D., Et-Touhami, M., Puffer, J., (2003). Cyclo-, magneto-, and bio-stratigraphic constraints on the duration of the CAMP event and its relationship to the Triassic-Jurassic boundary. *Geophysical Monograph Series.* 7–32. https://doi.org/10.1029/136gm02
59. Panchal, S., Shrivastava, A. K. (2022). Landslide hazard assessment using analytic hierarchy process (AHP): A case study of National Highway 5 in India. *Ain Shams Engineering Journal, 13*(3), 101626.
60. Petit, J.-P. (1976). La zone de décrochement du Tizi n'Test (Maroc) et son fonctionnement depuis le Carbonifère. *Thèse de 3e cycle, Université de Montpellier, France.* 272.
61. Petit, J.-P., S. Raynaud, and J.-P. Cautru (1985). Microtectonique cas sante lors du plissement d'un conglomérat (Mio-Pliocène du Haut Atlas; Maroc), *Bull. Soc. Géol. Fr. 1*(3), 415–421, https://doi.org/10.2113/ gssgfbull.i.3.415
62. Proust, F., Petit, J.-P., et Tapponnier, P. (1977). L'accident de Tizi n'Test et le rôle des décrochements dans la tectonique du Haut Atlas occidental (Maroc). *Bulletin de la Société géologique de France, XIX*(7), 541–551. https://doi.org/10.2113/gssgfbull.s7-xix.3.541
63. Qarbous, A.; Medina, F., Hoepffner, Ch. (2003). Le bassin de Tizi n'Test (Haut Atlas, Maroc): exemple d'évolution d'un segment oblique au rift de l'Atlantique central au Trias. *Canadian Journal of Earth Sciences, 40,* 949–964. https://doi.org/10.1139/e03-029
64. Qarbous, A., Medina, F., Hoepffner, C. (2008). Tectonique cassante et état de contrainte dans le bassin de Tizi n'Test (Haut Atlas, Maroc) au cours de l'inversion tertiaire. *Estudios Geológicos, 64*(1), 17–30. https://doi.org/10.3989/egeol.08641365
65. Qarbous, Q., Timoulali, T., Hoepffner, C., Chalouan, A., Ouzzaouit, L.A., Allaki, F., Bargach, K., (2025). Update on the Compressional Tectonic Evolution of the Tizi n'Test Fault Zone (Western High Atlas) and Its Relation to the Al-Haouz Earthquake of 8 September 2023. *Bulletin of the Seismological Society of America 2025;* https://doi.org/10.1785/0120240212
66. Ramli M. F.; Yusof. N; Yusoff M. K; Juahir. H; Shafri H. Z. M. (2010). Lineament mapping and its application in landslide hazard assessment: a review., *69*(2), 215–233. https://doi.org/10.1007/s10064-009-0255-5
67. Redouane, M., Mhamdi, H., Haissen, F., Raji, M. and Sadki, O. (2022). Lineaments extraction and analysis using Landsat 8 (OLI/TIRS) in the Northeast of Morocco. *Open Journal of Geology, 12,* 333–357. https://doi.org/10.4236/ojg.2022.125018
68. Rivera, C.A., Valqui-Reina, S.V., García-Naranjo, L.F., Ocaña-Zúñiga, C.L., Auquiñivin-Silva, E.A., Chapa-Gonza, S.R., Cieza-Tarrillo, D., Vergara, C.G., Vergara, A.J. (2025). Geospatial Landslide risk mapping using AHP and GIS: A case study of the Utcubamba River Basin, Peru. *Appl. Sci., 15,*

9423. https://doi.org/10.3390/app15179423

69. Roback, K., Clark, M. K., West, A. J., Zekkos, D., Li, G., Gallen, S. F., Chamlagain, D., Godt, J. W. (2018). The size, distribution, and mobility of landslides caused by the 2015 Mw7. 8 Gorkha earthquake, Nepal. *Geomorphology, 301,* 121–138.
70. Saaty, T. L. (1977). A scaling method for priorities in hierarchical structures. *J. Math. Psychol. 15*, 234–281. https://doi.org/10.1016/0022-2496(77)90033-5
71. Saaty, T. L., Vargas, L. G. (1980). Hierarchical analysis of behavior in competition: Prediction in chess. *Behav. Sci. 25,* 180–191. https://doi.org/10.1002/bs.3830250303
72. Sassa, K., Fukuoka, H., Wang, F., Wang, G. (2007). Landslides induced by a combined effect of earthquake and rainfall. Progress in Landslide Science. *Springer, Berlin, Heidelberg,* 193–207. https://doi.org/10.1007/978-3-540-70965-7_14
73. Serkhane, A., Saidi, Y., Oukid, F., Mehdadi, F., Djeddi, R., Rabah, Y. (2024). Cartographie de la susceptibilité aux glissements de terrain par les méthodes du rapport de fréquences (FR) et du poids de l'évidence (WoE) dans la wilaya de Mila. *Bulletin du Service Géologique de l'Algérie, 33*(1), 73–94.
74. Schaer, J.P. (1964). Volcanisme Cambrien dans le massif ancien du Haut Atlas occidental. *Comptes Rendus Academic Sciences, 258,* 2114–2117.
75. Sur, U., Singh, P., Meena, S. R. (2020). Landslide susceptibility assessment in a lesser Himalayan road corridor (India) applying fuzzy AHP technique and earth-observation data. *Geomatics, Natural Hazards and Risk, 11*(1), 2176–2209.
76. Tanyaş, H., van Westen, C. J., Allstadt, K. E., Anna Nowicki Jessee, M., Görüm, T., Jibson, R. W., Godt, J.W.,Sato, H.P, Schmitt, R.,G, Marc, O., Hovius, N. (2017). Presentation and analysis of a worldwide database of earthquake-induced landslide inventories. *Journal of Geophysical Research: Earth Surface, 122*(10), 1991–2015.
77. Tarboton, D. G., Bras, R. L., Rodriguez-Iturbe, I. (1991). On the extraction of channel networks from digital elevation data. *Hydrological Processes, 5*(1), 81–100. https://doi.org/10.1002/hyp.3360050107
78. Teixell, A., M.-L. Arboleya, M. Julivert, and M. Charroud (2003), Tectonic shortening and topography in the central High Atlas, Tectonics, 22(5), 1051, 1–6. https://doi.org/10.1029/2002TC001460
79. Thiery, Y., Terrier, M. (2018). Évaluation de l'aléa glissements de terrain: État de l'art et perspectives pour la cartographie réglementaire en France. *Revue Française de Géotechnique, (156)*3, 1–19. https://doi.org/10.1051/geotech/2019003
80. Tixeront, M. (1973). Lithostratigraphie et minéralisations cuprifères et uranifères syngénétiques et familières des formations détritiques permo-triasiques du couloir d'Argana. *Notes Mém. Serv. géol. Maroc, 33,* 249, 147–177.
81. Timoulali, T., Bouiflane, M., Bouskri, G., Azguet, R., El Fellah, Y. (2019). Lithosphere structures dynamics in the central High Atlas (Morocco) by seismic tomography and gravimetric data. *Geodesy and Geodynamics, 1–15,* https://doi.org/10.1016/j.geog.2019.01.005
82. Whipple, K. X., Tucker, G. E. (1999). Dynamics of the stream-power river incision model: Implications for height limits of mountain ranges, landscape response times, and research needs. *Journal of Geophysical Research: Solid Earth, 104*(B8), 17661–1767. https://doi.org/10.1029/1999jb900120
83. Wilson, M. F. J., O'Connell, B., Brown, C., Guinan, J. C., Grehan, A. J. (2007). Multiscale terrain analysis of multibeam bathymetry data for habitat mapping on the continental slope. *Marine Geodesy, 30*(1–2), 3–35. https://doi.org/10.1080/01490410701295962
84. Yalcin A. (2008). GIS-based landslide susceptibility mapping using analytical hierarchy process and bivariate statistics in Ardesen (Turkey): Comparisons of results and confirmations. *CATENA, 72*(1), 1–12. https://doi.org/10.1016/ j.catena.2007.01.003
85. Yeck, W. L., A. E. Hatem, D. E. Goldberg, W. D. Barnhart, J. A. Thompson Jobe, D. R. Shelly, A. Villaseñor, H. M. Benz, and P. S. Earle (2023). Rapid Source Characterization of the 2023 Mw 6.8 Al Haouz, Morocco, Earthquake, *The Seismic Record. 3*(4), 357–366, https://doi.org/10.1785/0320230040
86. Ziraoui, A., Kissi, B., Aaya, H., Mrabet, N., Azdine, I. (2024). Seismic risk assessment, damage estimation, and strengthening of seismic construction standards in Morocco. *Journal of Building Pathology and Rehabilitation, 9*(1), 79. https://doi.org/10.1007/ s41024-024-00437-z
87. Zühlke R., Bouaouda M.S., Ouajhain B., Bechstädt T., Leinfelder R. (2004). Quantitative Meso-/Cenozoic development of the east ern Central Atlantic continental shelf, western high Atlas, Morocco. *Mar Pet Geol 21*(2), 225–276. https://doi.org/10.1016/J.MARPETGEO.2003.11.014
88. United States Geological Survey Earth Explorer. https://earthexplorer.usgs.gov/
89. The Earthquake Catalogue of the National Geographic Institute (IGN). https://www.ign.es/web/ign/portal
90. Earthquake Hazards Program - Preferred Landslide Model. https://earthquake.usgs.gov/earthquakes/eventpage/us7000kufc/ground-failure/summary.
91. Business Performance Management Singapore (BPMSG) AHP Priority Calculator software. https://www.bpmsg.com